ELSEVIER

Earth and Planetary Science Letters 134 (1995) 441–457

EPSL

Breaking new ground: Estimates of crack depth along the axial zone of the East Pacific Rise (9°12′–54′N)

Dawn J. Wright [a,b,*], Rachel M. Haymon [a], Ken C. MacDonald [a]

[a] *Department of Geological Sciences and Marine Science Institute, University of California, Santa Barbara, CA 93106-9630, USA*
[b] *Department of Geosciences, Oregon State University, Corvallis, OR 97331-5506, USA*

Received 20 December 1994; accepted 3 May 1995

Abstract

Using simple fracture mechanics models, the depths of fissures that were observed along the axial zone of the East Pacific Rise (EPR) from 9°12′ to 54′N with the deep-towed *Argo I* vehicle are estimated. The widest cracks (~ 4–8 m) along this fast-spreading portion of the EPR are the deepest, and are spatially correlated with the broadest, youngest, and most hydrothermally active portions of the ridge crest. If the widest (deepest) cracks are not primarily eruptive, they should be most abundant in areas of older lava flows, having increased in width with time. This is not observed. Some of the widest cracks are located where the 1991 eruption of the ridge crest occurred at ~ 9°45′–52′N and may be deep enough to reach the sheeted dikes of Layer 2B. These cracks may have tapped melt during the eruption and facilitated the flux of vapor-rich hydrothermal fluids through overlying lava flows. The narrowest, presumably shallowest, cracks correspond to the narrowest, oldest, and least hydrothermally active portions of the ridge crest. We interpret the wide, deep cracks as primarily eruptive in origin, and suggest that they may be associated with the inflation of an axial magma chamber, whereas the narrow, shallow cracks are interpreted as primarily tectonic and are thought to be associated more with far-field plate stresses.

1. Introduction

When considering the effects of the cracking of an oceanic plate, the relevant crack parameters are crack length, spacing, width, depth, and variation of crack width as a function of depth [1,2]. Crack length and spacing are fairly easily determined from sides-can sonar surveys (e.g., [3–5]) and crack width can, in principle at least, be determined from near-bottom camera observations (e.g., [6,7]), although this has rarely been reported. The critically important parameters of crack depth and variation in crack width as a function of depth have never been determined anywhere on the seafloor and have only recently been perceived as important in marine geology [8]. The determination of these parameters must be a high priority for any study that hopes to understand the nature of extensional failure of the ocean crust [9,10].

The present study represents one of the first attempts at estimating crack depth for fissures along the axis of a seafloor spreading center. Absolute crack depth and along-strike variation in crack depth are estimated from the *widths* of fissures that were

* NOAA—Pacific Marine Environmental Laboratory, Hatfield Marine Science Center, 2115 SE, OSU Drive, Newport, OR 97365, USA

SSDI 0012-821X(95)00081-X

observed by *Argo I* in 1989 along the axial zone of the East Pacific Rise (EPR) from 9°12′ to 9°54′N [7] (Figs. 1 and 2). Wright et al. [7] used video and sonar observations from the deep-towed *Argo I* optical/acoustic imaging system to establish the abundance, spatial distribution, and widths (Fig. 3) of these fissures, as well as the relative age distribution of lava flows, along a narrow (< 500 m wide) ~ 80 km long corridor of the ridge crest. In this study, the along-axis variation in the depths of these fissures are reported with confidence because of the variation in their widths observed by Wright et al. [7]. However, the absolute depths of these cracks can only be speculated upon, using the best available models from fracture mechanics.

Ninety percent of the fissures used in this study (i.e., 719 out of 795) are cracks detected by the *Argo I* video camera. The *Argo I* video camera has a smaller field of view than the *Argo I* sidescan sonar, and can resolve features as small as ~ 10 cm–1 m in width [11]. Therefore, for this study the inferred along-strike variation in depth and absolute depth (average and maximum) are reported only for those fissures detected by the *Argo I* video because the

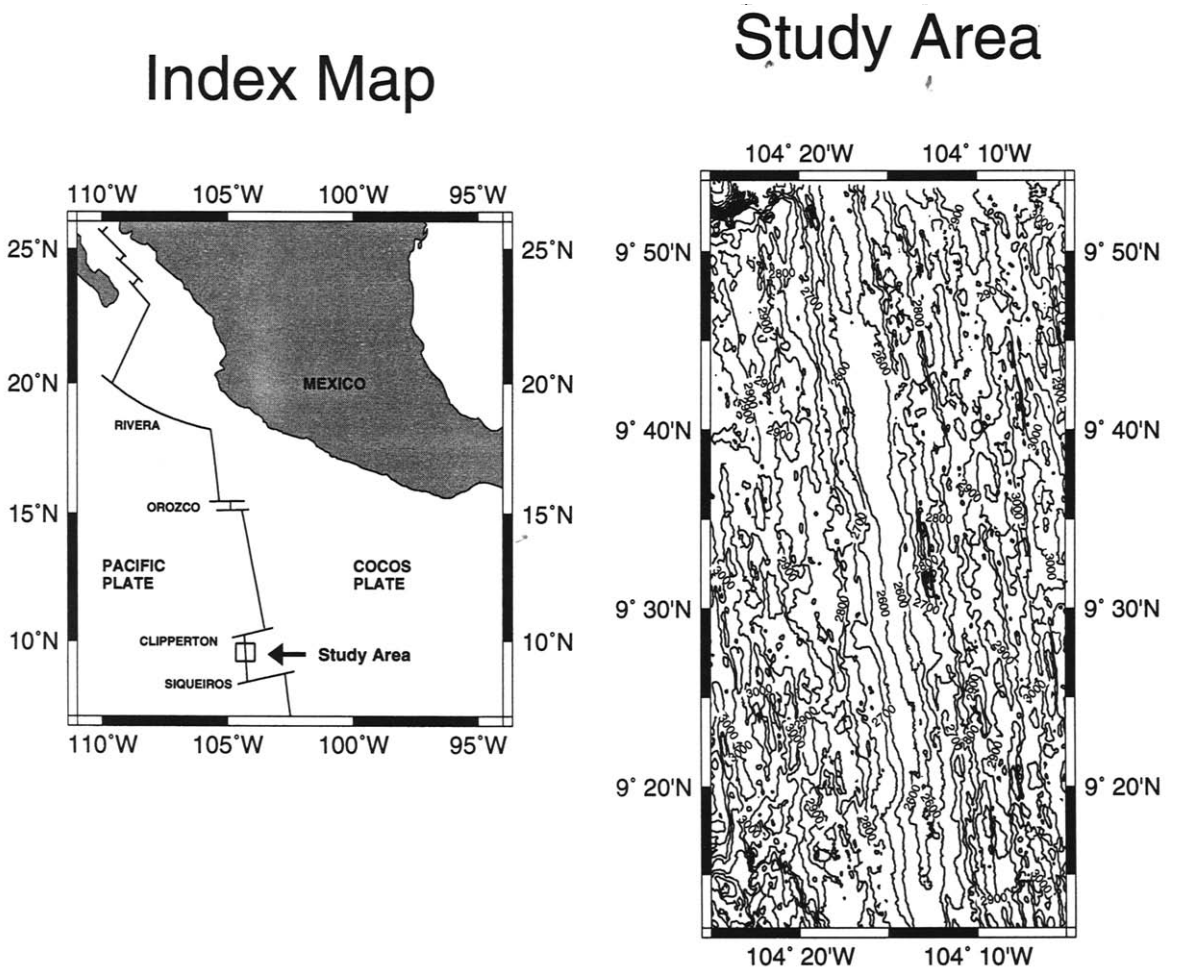

Fig. 1. Location of the study area and regional bathymetry. Inset map shows the location of the study area on the northern EPR. Sea Beam bathymetry is from Wilcock et al. [49]. Contour interval is 50 m. The study area covers a narrow (< 500 m wide) zone of the ridge crest from 9°12′ to 54′N. Full opening rate is 11 cm/yr [50].

video yields a more accurate determination of fissure width. Fissures detected by the video system in the study area range in width from 10 cm to 8 m, with an average width of 2.5 m [7] (Fig. 3a). It should be noted that fracture width and length usually have a log-normal or power-law distribution, so the arithmetic mean is not always a good indication of the most common value). The *Argo I* sidescan sonar yields a more accurate determination of fissure length due to its larger swath (it maps features of the order of ~50–100 m long despite the crabbing of the *Argo I* vehicle [11] [D. Fornari, pers. commun., 1994]). The *Argo I* sidescan sonar analog records did not yield fissure widths of the necessary accuracy for this study.

Calculations of absolute crack depth assume that oceanic basement is a uniform, isotropic, elastic medium. Sempéré and Macdonald [12] and Pollard and Aydin [13] used this assumption successfully in modelling the geometry and propagation of overlapping spreading centers, which were treated as initially parallel elastic cracks. Rigorous analytical solutions that relate crack width to crack depth for three-dimensional, semi-elliptical surface cracks are not yet available [A. Gudmundsson, pers. commun., 1992]. A few *two-dimensional* solutions exist, such as the subaerial models adapted in this study to the mid-ocean ridge environment [14–16].

The models in this study are based on the plausible assumption that the crack walls deform in a linearly elastic manner. The applicability of these models to the ocean crust along the EPR axis is particularly sensitive to the elastic properties of the crust [A. Rubin, pers. commun., 1993], which have yet to be determined in situ. Seismic velocity, electrical resistivity or deep borehole investigations (e.g., borehole televiewer studies such as those of Zoback and Anderson [17]) may eventually be adequate to determine the actual depth distribution of these cracks and thus evaluate and test the estimates in this study. However, until in-situ determinations or a rigorous three-dimensional analytical solution for anisotropic, heterogeneous ocean crust become available, one must rely on a two-dimensional solution, using reasonable values for the linear elasticity properties or parameters and density of the rock. These two-dimensional models rest on a substantial body of experimental information obtained with rocks, metals, plastics, glass and concrete, and have met with success in subaerial studies and engineering applications.

2. Elastic moduli for the EPR crest (9°12′–54′N)

For the complete specification of a linear elastic material, any two of the elastic moduli (λ, Lamé's constant; G, the shear modulus (rigidity); ν, Poisson's ratio; E, Young's modulus; K, the bulk modulus) must be known [2]. For the models employed in this study, Poisson's ratio is used either with Young's modulus or with the shear modulus.

2.1. Poisson's ratio

The dynamic Poisson ratio can be calculated from seismic compressional (V_p) and shear wave (V_s) velocities. From these dynamic moduli, the static moduli, which should be used in the crack models presented below, can often be inferred. However, because direct shear wave velocity measurement in young ocean crust is difficult, especially in the uppermost part of the crust, the dynamic Poisson ratio is largely unknown [18]. One is therefore compelled to rely on a static Poisson ratio determined from laboratory measurements of basalt as an approximation of the in-situ value. The commonly assumed Poisson ratio for oceanic crust, based on the laboratory measurements of Christensen [19], is 0.3 (yielding $V_p/V_s = 1.9$). However, the amplitude modeling of the on-bottom seismic refraction data of Christeson et al. [20] near 9°30′N indicates a Poisson ratio at the seafloor of at least 0.43 (i.e., $V_p/V_s > 3$). This value is similar to other determinations of Poisson's ratio for young oceanic crust, which fall in the range 0.39–0.46 [21–23]. These higher values of Poisson's ratio are more common for material dominated by thin cracks (i.e., aspect ratios much less than one) than by material dominated by more equidimensional voids, such as vesicles or interpillow voids [2,24]. For this study, a Poisson ratio of 0.43 is adopted as the preferred value (Table 1). We also evaluate the consequences of using a Poisson ratio of 0.48, which is the preferred value of Christeson et al. [20], based on high-resolution seismic measurements in our study area.

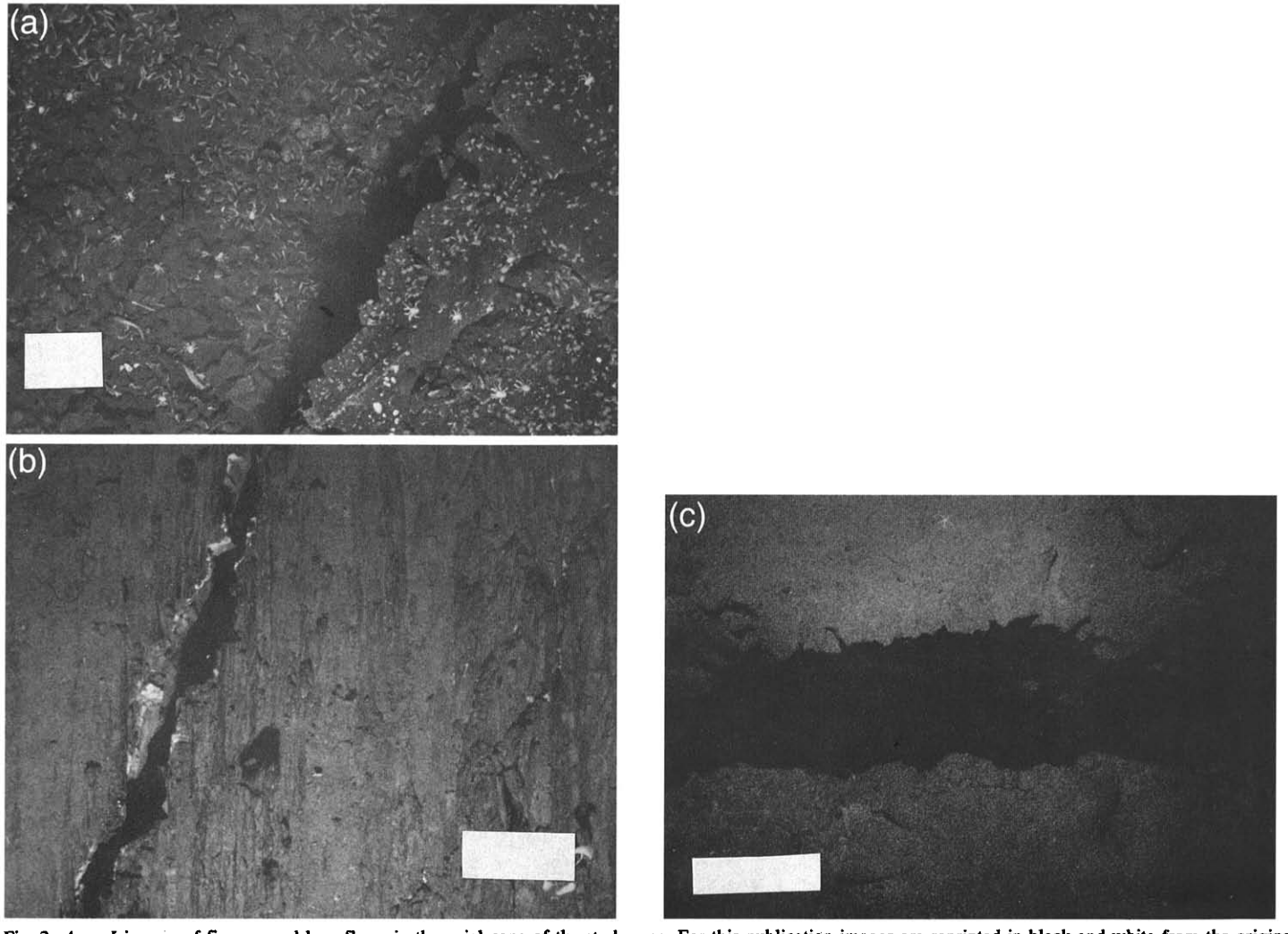

Fig. 2. *Argo I* images of fissures and lava flows in the axial zone of the study area. For this publication images are reprinted in black and white from the original color film. Scale bar is 1 m in images (A–C) and 5 m in images (D–F). (A) 35 mm photograph of a hydrothermally active, 0.5 m wide fissure in a relatively young (Age 1) autobrecciated sheet flow along the axial zone of EPR 9°49′N. White specks in photograph are dense communities of mussels, clams and galatheid crabs, which provide evidence of hydrothermal discharge. Depth ~2550 m, altitude ~6.0 m, heading ~10°. (B) 35 mm photograph of a ~0.3 m wide fissure in a relatively older (Age 2) sheet flow along the axial zone of EPR 9°22′N. Depth ~2574 m, altitude ~5.0 m, heading ~10°. (C) 35 mm photograph of a ~1 m wide fissure in a relatively old (Age 3) sheet flow along the axial zone of EPR 9°25′N. Depth ~2590 m, altitude ~4.0 m, heading ~270°. (D) Electronic still camera image of a 5 m wide (on left) and a 2 m wide (on right) fissure in older (Age 2) sheet flows just outside the axial zone of EPR 9°50.0′N, 104°20.1′W. Depth ~2600 m, altitude ~6.0 m, heading ~340°. (E) Video image (forward-looking) of 6 m wide fissure in a young (Age 1) lobate flow along the axial zone of EPR 9°53.0′N. Depth ~2536 m, altitude ~6.2 m, heading ~350°. Scale bar applies to the foreground in this image. (F) Video image of 5 m wide fissure in older (Age 2) sheet flow along the axial zone of EPR 9°38.6′N. Depth ~2551 m, altitude ~6.3 m, heading ~350°.

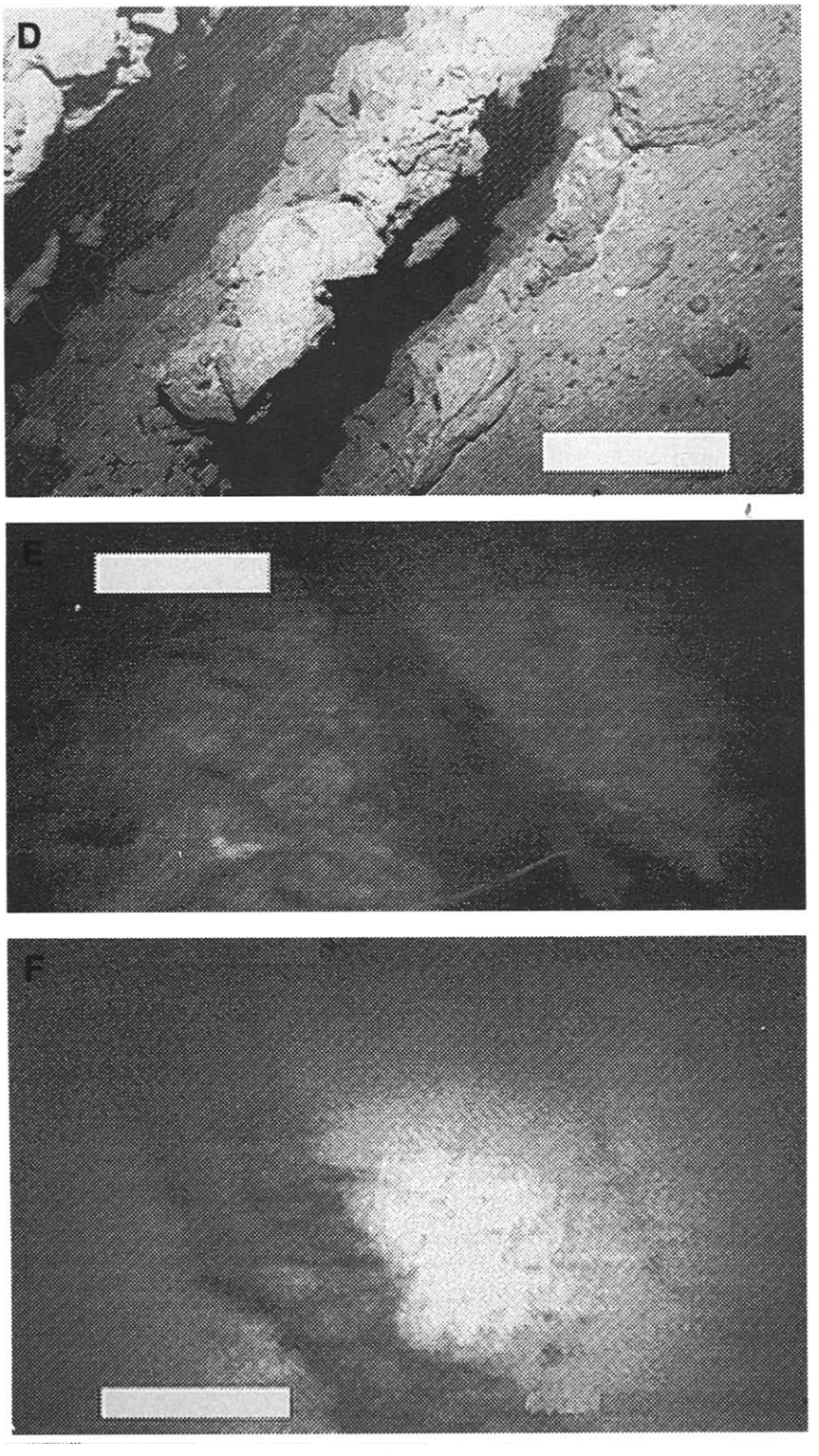

Fig. 2 (continued).

2.2. Young's modulus and shear modulus

Dynamic Young's modulus, E_d, is given by Jaeger and Cook [2] as:

$$E_d = V_p^2 \rho \frac{(1+\nu)(1-2\nu)}{(1-\nu)} \quad (1)$$

where V_p is P-wave velocity, ν is Poisson's ratio and ρ is rock density. For the purpose of this study, V_p is the average P-wave velocity and ρ is the average rock density of the uppermost 1 km of crust at the EPR 9°12′–54′N. The relationship between E_d and static Young's modulus (E_s) is somewhat complex and depends on the rock in question [25]. In general, because cracks propagate much more slowly than the velocities of seismic waves, static Young's modulus should be used [26,27]. In laboratory measurements the E_d/E_s ratio is commonly around 2.0 [25], but for in-situ measurements this ratio ranges from 1.5 to 9.1 for common extrusive rocks [27]. Because in-situ measurements in the Tertiary and

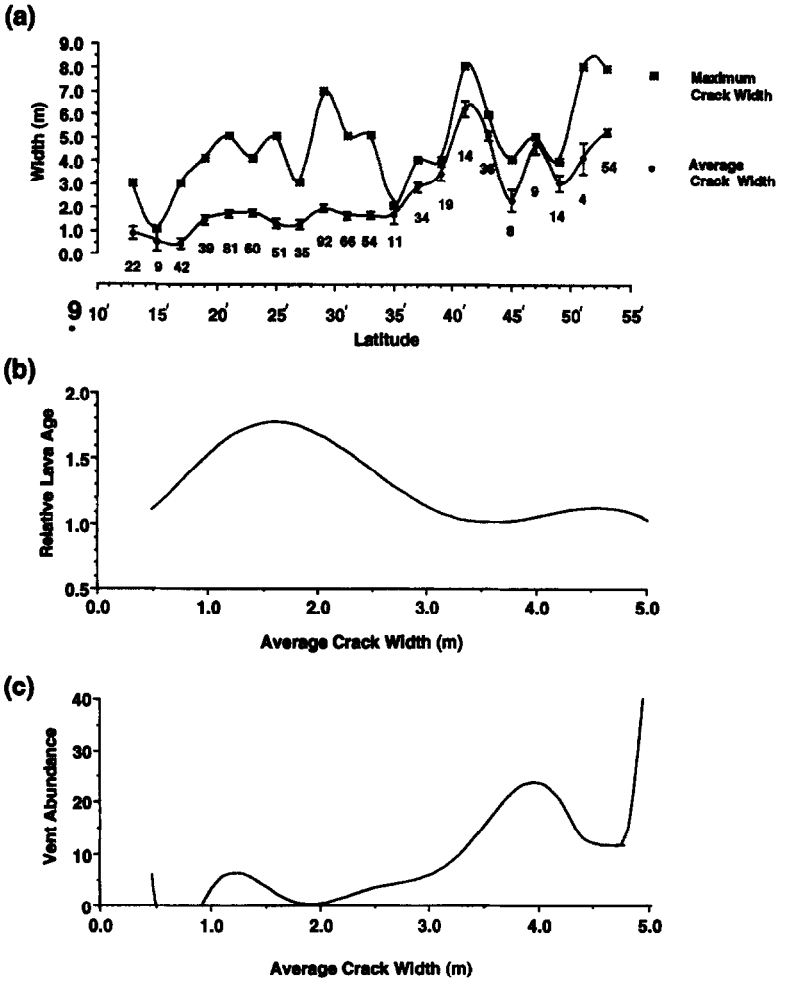

Fig. 3. (a) Interpolated profiles of average and maximum crack width measured in bins of 2 minute latitude along-strike. Data are from Wright et al. [7]. Error bars represent the standard errors (i.e., standard deviations of the mean) within each bin. Numbers below the profiles are the number of observations per bin. (b) Interpolated profile of relative lava age vs. average crack width. Difficulties inherent in accurately determining lava ages are discussed in Wright et al. [7]. Because of this source of error, it is important to consider the overall trend in the curve rather than its actual shape. (c) Interpolated profile of hydrothermal vent abundance vs. average crack width.

Quaternary lava piles of Iceland suggest a ratio of 2.0 [28], the E_d/E_s ratio adopted for this study is also 2.0. For this study, E_d is calculated using values for V_p, ρ and ν from Table 1, and values for E_s are then estimated from E_d using the ratio of 2.0. The subscript on E is hereafter omitted. A static shear modulus is also calculated (Table 1) using the formula of Jaeger and Cook [2]:

$$G_s = \frac{E}{2(1+\nu)} \quad (2)$$

3. Crack depth models

Fracture mechanics provides a fundamental relation for estimating tensile crack depth from tensile crack width in a volcanic rift zone environment [29]:

$$\text{Crack depth} \propto \frac{\text{elastic moduli} * \text{displacement}}{\text{tectonic stress}} \quad (3)$$

where displacement can be taken to be the width of the crack at the surface and tectonic stress is essentially the applied tensile stress (Fig. 4). This relation depicts a 'top down' mode of cracking where the crack initiates at the surface and the depth of penetration is related to the width of opening. The crack is therefore not magma filled, but can of course serve as a conduit for upwardly propagating magma and hydrothermal fluids. Few specific models of this sort have been proposed in the geophysical literature, and the two models employed in this study represent the bulk of that which is available for applications to volcanic rift zones. Most published models come from engineering and apply to hydraulically induced fractures in oil and gas wells (e.g., [1]) or to microfractures in building materials (e.g., [30]).

3.1. Model 1

Model 1 is based on the formulation by A. Rubin [pers. commun., 1993], the theory of which relies on

Table 1
Elastic moduli and related parameters used in calculations

Parameter	Definition	Value	Units	References
b	Thickness of crust on axis	1200 ± 200	m	[37,38]
E	Static Young's modulus	***9700 ± 1000 (ν = 0.43)***	MPa	This study
		3100 ± 1000 (ν=0.48)	MPa	This study
g	Acceleration of gravity	9.8	m/s^2	
G	Static shear modulus	***3400 ± 1000 (ν=0.43)***	MPa	This study
		1100 ± 1000 (ν=0.48)	MPa	This study
T_0	Rock tensile strength	3 +3/-2	MPa	[14,35]
$V_1(d/b)$	Tada's stress function	2.56 (1.52 in Iceland)		This study [14]
V_p	Avg. P-wave velocity of uppermost 1 km	4600 ± 400	m/s	[23]
w	Crack width	0.1 - 8.0	m	This study
z_{max}, d	Maximum depth of absolute tension	400 ± 100 (800 ±100 in Iceland)	mbsf	This study [35]
z_0	Crack depth	60 - 500 ± 40	mbsf	This study
υ	Poisson's ratio	***0.43***		[20]
		0.48		[20]
ρ	Avg. rock density of uppermost 1 km	2600 ± 100	kg/m^3	[23]
σ	Tensile stress at time of crack formation	30 ± 10 (25 ± 10 in Iceland)	MPa	[34] [46]

Our preferred values for Poisson's ratio, Young's modulus and shear modulus are ***italicized***.

the studies of Rubin and Pollard [31] and Rubin [15]. These studies model dikes and faults as internally pressurized planar cracks that propagate in a three-dimensional halfspace due to dilation by fluid injection. Unlike the 'top down' mode described earlier, most of these cracks initiate at depth and propagate both up and down as they lengthen. In Model 2, crack depth, z_0, is proportional to the ratio of tensile stress, σ, to the crack halfwidth $(w/2)$ and the elastic stiffness of the host rock, defined as $G/(1-\nu)$ in Rubin [32], Lister and Kerr [33] and Rubin [15]:

$$z_0 = \frac{(G/(1-\nu))(w/2)}{\sigma} \tag{4}$$

A value of 30 MPa for σ is adopted based on Lachenbruch [34] (Table 1). Using adopted values for G and ν (Table 1), an elastic stiffness for the EPR at 9°12′–54′N is estimated to be ~ 6000 MPa, which is close to the Icelandic value of 5000 MPa [A. Gudmundsson, pers. commun., 1995]. The EPR value also falls within the range of 2000 and 11,000 MPa as determined by Lister and Kerr [33] and Rubin [32] respectively. Lister and Kerr [33], in considering both continental and oceanic crust, estimated an elastic stiffness of ~ 2000 MPa based on laboratory measurements of G and ν for granite (G = 1000–2000 MPa and $\nu = 0.1$) and basalt (G = 2500–3000 MPa and $\nu = 0.22$–0.28). Rubin [32] derived an elastic stiffness of ~ 11,000 MPa for the

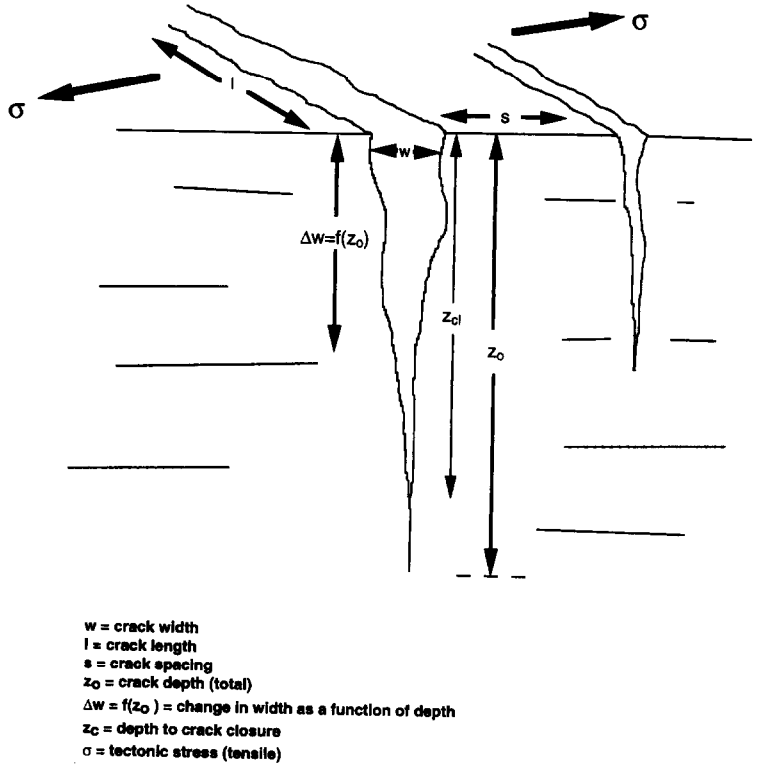

Fig. 4. Illustration of the relevant parameters involved in considering the effects of cracking on the properties of an igneous crustal plate. Symbols are defined in the illustration. The fracture mechanics models proposed in this study are concerned mostly with the parameters w (crack width), z_0 (crack depth) and σ (tensile stress).

uppermost 1 km of Icelandic crust, based on seismic refraction data and assuming $\nu = 0.25$ (the elastic stiffness for shallow Hawaiian crust is estimated to be ~ 4000 MPa [32]). In testing how sensitive the predictions of Model 1 are to the assumed elastic stiffness, crack depths calculated with an elastic stiffness of ~ 2500 MPa (i.e., $G = 2000$ MPa and $\nu = 0.22$) are almost equal to depths calculated with an elastic stiffness of ~ 6500 MPa (i.e., $G = 3400$ and $\nu = 0.48$).

3.2. Model 2

Unlike Model 1, Model 2 assumes a crack of finite dimensions. In this case, the width of the crack may be controlled by either its depth or its length (Fig. 4). In order to know which is the minimum or width-controlling dimension, Model 2 draws on the following reasoning of Gudmundsson and Bäckström [14], Gudmundsson [35] and A. Gudmundsson [pers. commun., 1992]: (1) Use the Griffith crack criterion [36] to estimate the maximum possible depth of absolute tension in the crust; (2) compare this depth with an estimate of average length for the cracks under consideration (in the case of this study, the estimate must be derived from the *Argo I* sidescan sonar observations); (3) if cracks are generally longer than this depth, then the crack depth is the minimum and thus width-controlling dimension, and Model 2 applies. This procedure is very appropriate for the study as a rigorous width-to-depth relation is needed.

Griffith developed a theory of fracture strength based on the assumption that minute internal and surface cracks exist throughout a material [36]. His theory assumes that fracture initiation occurs from the points of highest tensile stress on surfaces of microscopic flaws, or 'Griffith's cracks', in brittle material (in a biaxial stress field). Joints, lava flow contacts and tension cracks may be regarded as the macroscopic analogy to Griffith's cracks [14]. If σ_1 is the greatest compressive stress, σ_3 the least compressive stress and T_0 the tensile strength of the rock, the two-dimensional Griffith crack criterion for crack initiation is [2,36]:

$$\text{If } \sigma_1 < -3\sigma_3, \text{ then } \sigma_3 = -T_0 \tag{5}$$

$$\text{If } \sigma_1 > -3\sigma_3, \text{ then } (\sigma_1 - \sigma_3)^2 = 8T_0(\sigma_1 + \sigma_3) \tag{6}$$

Eq. (5) applies to the tensile regime whereas Eq. (6) applies to compression. Substituting $-T_0$ for σ_3 in Eq. (5) gives:

$$\sigma_1 \leq 3T_0 \tag{7}$$

If

$$\sigma_1 = \rho g z \tag{8}$$

[29] then:

$$T_0 = \frac{\rho g z}{3} \tag{9}$$

and solving for depth z gives:

$$z_{max} = \frac{3T_0}{\rho g} \tag{10}$$

where z_{max} is the maximum depth of absolute tension in the crust. Gudmundsson and Bäckström [14] report an average z_{max} of 500 m for Holocene fissures in the rift zone of Iceland and find that most large-scale tension cracks should develop into normal faults at crustal levels deeper than 500–800 m. Using the values in Table 1 yields a z_{max} of 400 ± 100 m for EPR 9°12′–54′N.

The length of fissures in the study area ranges from ~ 30 to ~ 650 m, with an average length of ~ 166 m, based on the *Argo I* sonar data of Wright et al. [7]. Many of the cracks are in general rubble filled, and many, if not most, of the shorter cracks are parts of arrays, with the distances between the ends of the cracks being much shorter than the lengths of the cracks themselves. These arrays behave in a mechanical fashion essentially as a single crack. It is therefore surmised that the cracks in the study area are generally longer than z_{max}, the inferred maximum depth of absolute tension. One may then use the following variation on the plane-stress model of Tada et al. [16] and Gudmundsson and Bäckström [14] (i.e., Model 2):

$$z_o = \frac{Ew}{\sigma V_1(d/b)} \tag{11}$$

where $V_1(d/b)$ is the stress function of Tada et al. [16], which has 1% accuracy for any d/b:

$$V_1(d/b) = \frac{1.46 + 3.42\left[1 - \cos\left(\frac{\pi}{2}\right)\frac{d}{b}\right]}{\left[\cos\left(\frac{\pi}{2}\right)\frac{d}{b}\right]^2} \tag{12}$$

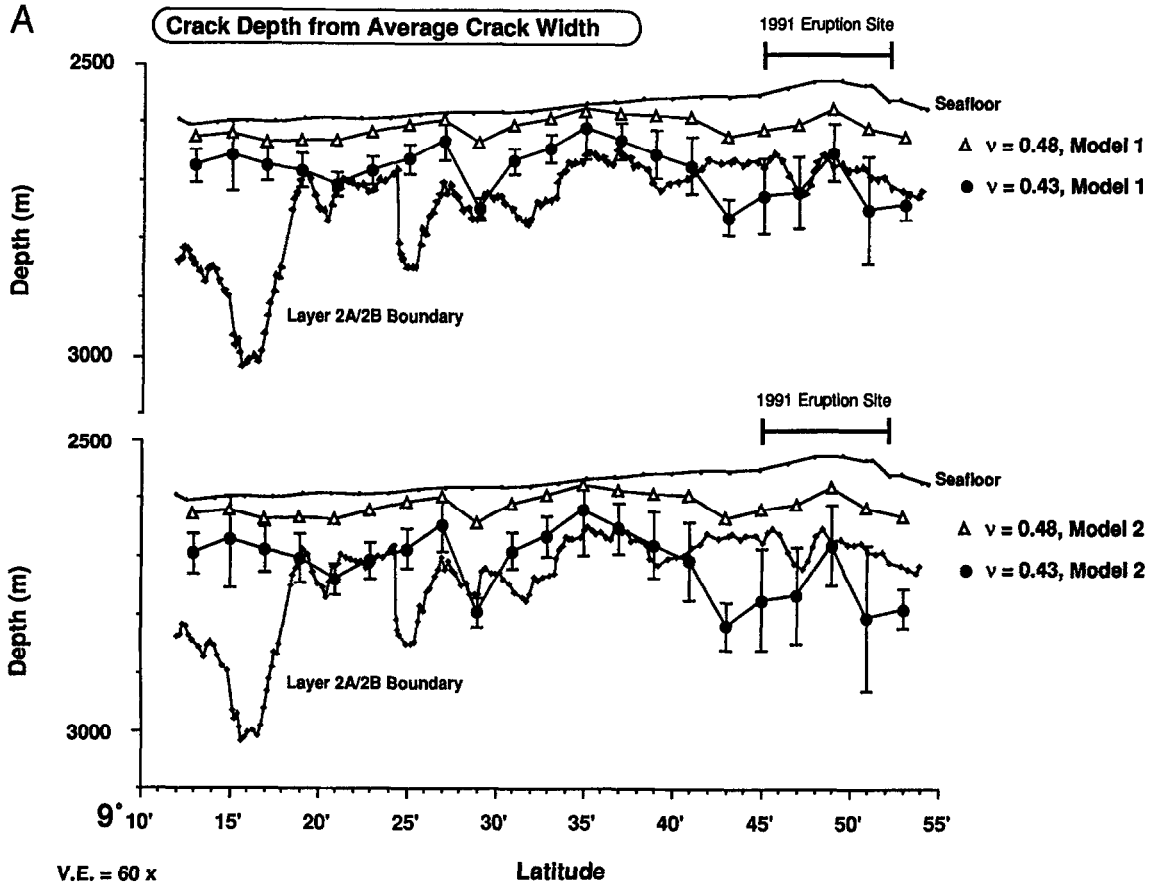
A
Crack Depth from Average Crack Width
1991 Eruption Site
Seafloor
ν = 0.48, Model 1
ν = 0.43, Model 1
Layer 2A/2B Boundary
Depth (m)
2500
3000
1991 Eruption Site
Seafloor
ν = 0.48, Model 2
ν = 0.43, Model 2
Layer 2A/2B Boundary
9°10' 15' 20' 25' 30' 35' 40' 45' 50' 55'
V.E. = 60 x
Latitude

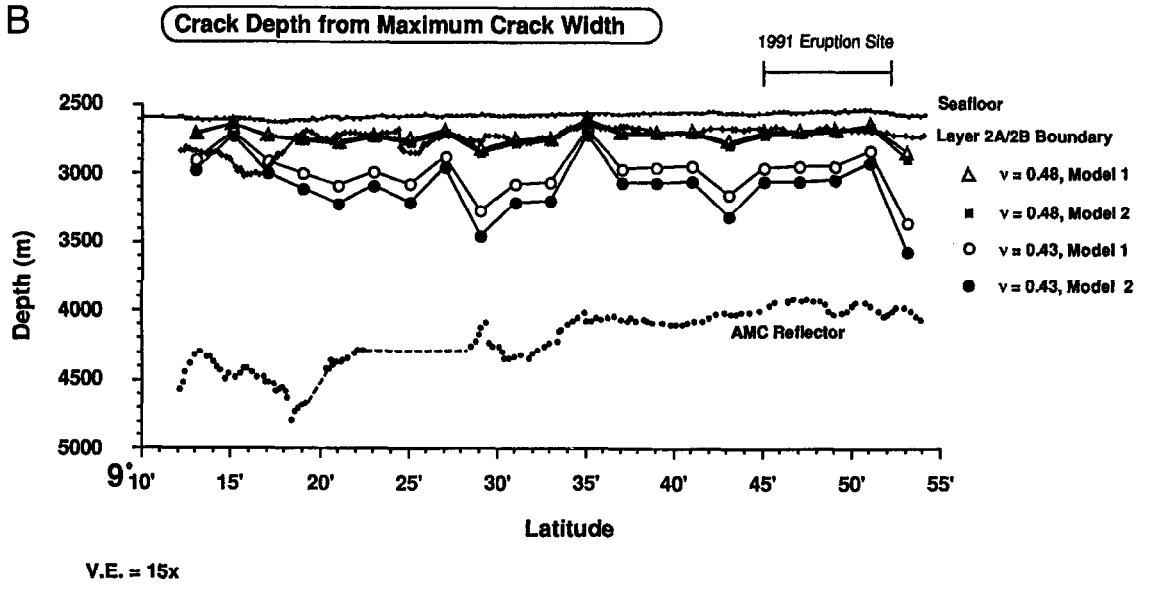
B
Crack Depth from Maximum Crack Width
1991 Eruption Site
Seafloor
Layer 2A/2B Boundary
ν = 0.48, Model 1
ν = 0.48, Model 2
ν = 0.43, Model 1
ν = 0.43, Model 2
AMC Reflector
Depth (m)
2500
3000
3500
4000
4500
5000
9°10' 15' 20' 25' 30' 35' 40' 45' 50' 55'
Latitude
V.E. = 15x

In the stress function above, d is 400 m, in accordance with the earlier estimate of z_{max}, and b is the brittle thickness of the crust, which would be the depth to the 600° isotherm on a fast-spreading axis. This translates to ~ 1200 m for the EPR at 9–10°N [37] (Table 1). The average depth to the axial magma chamber (AMC) reflector for the EPR at 9–10°N is just below this at ~ 1600 m [38] (Fig. 5).

An additional consideration regarding our estimates of crack depth involves the possible effects of pore-fluid pressure on crack formation. This is not considered in the present study but will be taken into account in future research. The present study assumes a rock tensile strength of ~ 3 MPa (Table 1), which is the best value currently available for volcanic rift zone environments. Nevertheless, this has an inaccuracy of a factor 2. The tensile strength, as mentioned before, may range from 1 to 6 MPa (Table 1), which would clearly cover the possible inaccuracy in ignoring potential effects of fluid pressure. Given reasonable values for the grain density and porosity of oceanic basalt (~ 3.0 g/cm^3 and ~ 0.01–0., respectively), one would arrive at a maximum depth of absolute tension of ~ 600 m, instead of the ~ 400 m cited earlier. The 400 m applies to dry rock (using our preferred density of 2600 kg/m^3 and a rock tensile strength of 3 MPa). It is not clear whether other factors, such as the effects of seawater pressure on crack propagation, need to be taken into account. The general effect of pore-fluid pressure is to increase the *probability* of failure in a rock [2]. Pore-fluid pressure affects only the normal stress, not the shear stress [A. Gudmundsson, pers. commun., 1995].

4. Crack depth estimates and interpretations

Fig. 5 shows the estimates of along-strike crack depth variation and absolute depth using both Model 1 and Model 2 for ν's_of 0.43 and 0.48. Also shown are the depths to the seafloor, the base of seismic Layer 2A (Fig. 5A), and the AMC reflector (Fig. 5B). The Layer 2A and AMC profiles were digitized from the two-way travel times of Harding et al. [39] and Kent et al. [38], and were converted to depth using the ridge crest velocity function of Vera et al. [23] (expanding spread profile (ESP) #5). ESP #5 currently provides the most detailed and reliable determination of the deeper velocity structure of the crust at the ridge axis for the 9°N region. Particular attention was paid to the gradients in velocity of the Vera et al. [23] model in zones approximately 160 m thick below Layer 2A and approximately 375 m thick above the AMC. Along-axis travel time to depth conversions were also cross-checked at various points along the axis with the common depth point (CDP) lines of Kent et al. [38] that were run across-axis. Vera and Diebold [40] provide travel-time-to-depth conversions for the seafloor, the base of Layer 2A and the top of AMC between 9°38′N and ~ 10°9′N, using more detailed seismic velocity information from iterative travel time forward modeling of key CDP gathers. Their depth estimates are therefore used in the section from 9°38′N to 9°54′N (Fig. 5B). The discontinuous behavior of the AMC reflector, especially between 9°22′N and 9°28′N (Fig. 5B), is related to a wandering shiptrack, a narrow magma chamber and a high lateral velocity variation in the uppermost crust of the ridge axis [38,39]. It should

Fig. 5. (A) Estimates of along-strike crack depth based on the *average* widths of fissures using two different values for Poisson's ratio, ν (see text; 0.43 is the preferred ν). Error bars are on the depth profiles calculated with a preferred ν of 0.43, and they represent the standard errors (i.e., standard deviations of the mean). The magnitude of the errors for the depth profiles calculated with a ν of 0.48 is approximately the same. The seafloor profile is from the Sea Beam bathymetry of Macdonald et al. [5]. The Layer 2A/2B boundary profile was converted from the two-way travel times of Harding et al. [39], Kent et al. [38] and Vera and Diebold [40]. The depth of the Layer 2A/2B boundary increases toward 9°20′N due to ship wander [38,39]. Vertical exaggeration is 60 ×. Bounds of the 1991 eruption site [42] are shown above. (B) Estimates of along-strike crack depth based on the *maximum* widths of fissures using two different values for ν. The seafloor and Layer 2A/2B boundary profiles are the same as in (A). The AMC reflector profile was converted from the two-way travel times of Harding et al. [39] and Kent et al. [38]. The dashed portion of the AMC reflector is in part due to ship wandering relative to the edge of the AMC [38,39]. The depth of the AMC increases toward 9°20′N due to ship wander [38,39]. Vertical exaggeration is 15 ×.

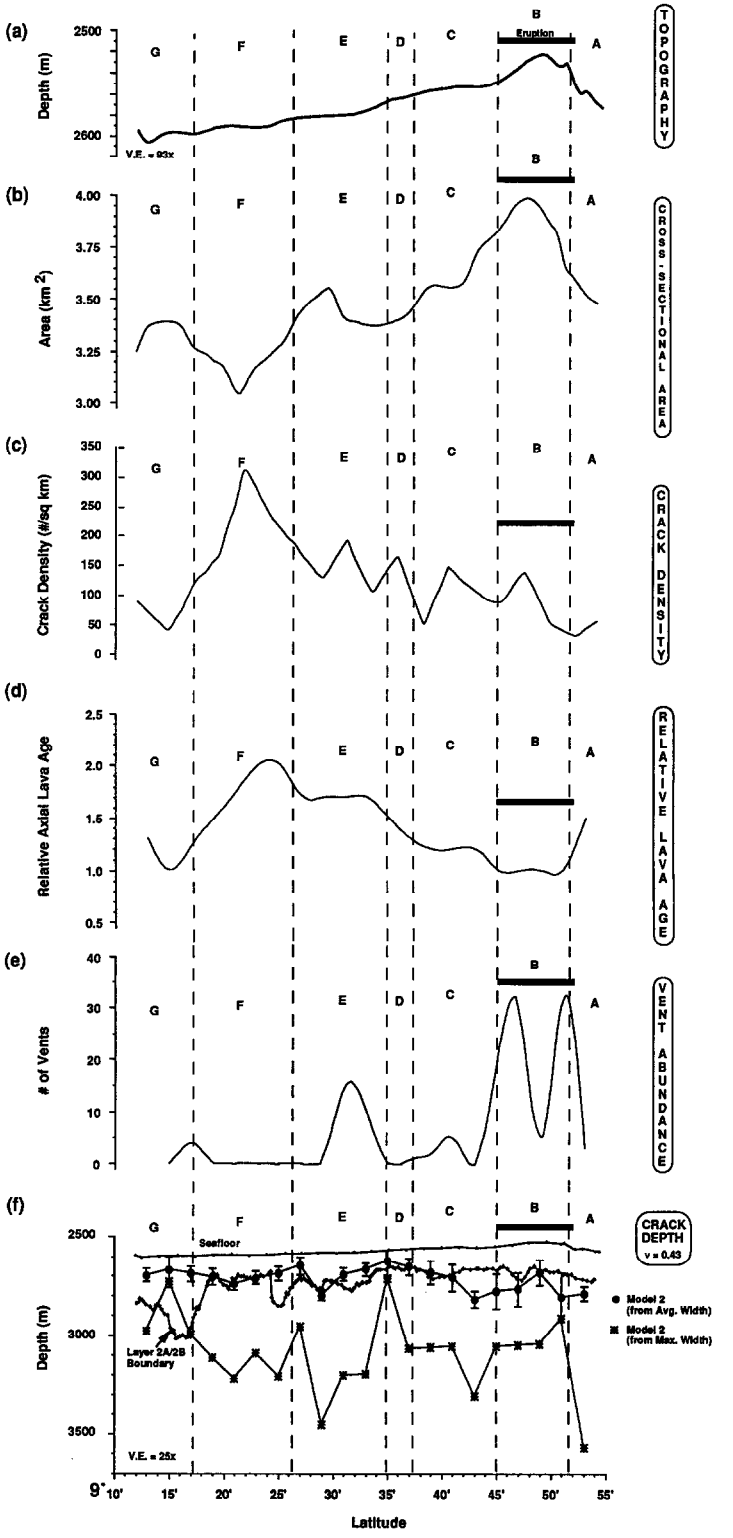
(a)
Depth (m)
2500
2600
V.E. = 93x
G
F
E
D
C
B
Eruption
A
TOPOGRAPHY
(b)
Area (km 2)
4.00
3.75
3.50
3.25
3.00
CROSS-SECTIONAL AREA
(c)
Crack Density (#/sq km)
350
300
250
200
150
100
50
0
CRACK DENSITY
(d)
Relative Axial Lava Age
2.5
2.0
1.5
1.0
0.5
RELATIVE LAVA AGE
(e)
# of Vents
40
30
20
10
0
VENT ABUNDANCE
(f)
Depth (m)
2500
3000
3500
Seafloor
Layer 2A/2B Boundary
V.E. = 25x
CRACK DEPTH
v = 0.43
Model 2 (from Avg. Width)
Model 2 (from Max. Width)
9°10'
15'
20'
25'
30'
35'
40'
45'
50'
55'
Latitude

also be noted that the center of the AMC reflector is displaced ~ 1–4 km to the west of the ridge axis between ~ 9°30′N and the 9°03′N overlapping spreading center [38,41].

4.1. Estimates of crack depth

For crack depths derived from the *average* crack width (i.e., the average widths of fissures within bins every 2 minutes of latitude along-strike; Fig. 5A), Model 1 with a preferred Poisson ratio, ν, of 0.43 predicts crack depths ranging from ~ 50 to 215 m with an uncertainty for each value of ± 30 m; Model 2 predicts depths between ~ 60–275 ± 40 m. Cracks which may penetrate the Layer 2A/2B boundary are located north of 9°42′N, where crack widths are the greatest (Fig. 3a). These cracks are also located where the 1991 eruption of the ridge crest occurred at ~ 9°45′–52′N [42]. The reader is reminded that the *Argo I* survey was completed in 1989, before the eruption. In testing how sensitive the predictions of models were to the shallow seismic velocity/density of the crust, the density was varied between 2.3 and 2.7 km/g and the velocity between 2000 and 5000 m/s. The models still predicted that the cracks in the region would penetrate the Layer 2A/2B boundary. In general, these crack depths are comparable to the crack depths directly observed in the eroded Tertiary and Pleistocene lava piles of the rift zone in southwest Iceland [28,43], and to those inferred for the Holocene pahoehoe lava flows of the rift zone in northeast Iceland [14]. Most of these Icelandic cracks range in depth from 200 to 400 m, and some are as deep as 1100 m below the surface of the rift zone [A. Gudmundsson, pers. commun., 1995].

For crack depth derived from *maximum* crack width (i.e., the maximum width of fissures in each of the 2 minute latitudinal bins along-strike; Fig. 5B), Model 1 with a preferred Poisson ratio of 0.43 leads to estimates of crack depths of the order of ~ 100–800 m below the seafloor; for Model 2, depths are of the order of ~ 100–1000 m below the seafloor. The depths of many of these are well within Layer 2B and exceed the estimate of the maximum depth of absolute tension for this portion of the EPR. Studies by Embley and Wilson [44] and Johnson [8] suggest that such depths are indeed feasible for a mid-ocean ridge environment. For example, SeaMARC II coverage of the northern wall of the Blanco Trough, south of the Juan de Fuca Ridge, reveals individual sidescan reflectors, which are visible as tension cracks at the surface, that can be followed down the face of the wall to a depth of over 1200 m within the crust [8].

4.2. Along-axis variation in crack depth

In general, the widest (4–8 m) deepest cracks occur along the broadest, youngest, most hydrothermally active portions of the ridge crest where crack density is low (Fig. 6b,c,d,f). The narrowest (< 4 m), shallowest cracks are found along the narrowest,

Fig. 6. Correlation of along-strike crack depth with along-strike axial topography, axial cross-sectional area, crack density, relative axial lava age and hydrothermal vent abundance for the EPR crest, 9°12′–54′N. Vertical dashed lines mark the latitudes of fourth-order ridge axis discontinuities as determined by Haymon et al. [48]. Fourth-order segments are lettered A–F after Haymon et al. [48] and Wright et al. [7]. Horizontal bars mark bounds of the 1991 eruption site [42]. (a) Seafloor topography from the Sea Beam bathymetry of Macdonald et al. [5]. Vertical exaggeration is 93 ×. (b) Smoothed along-strike variation in ridge axis cross-sectional area digitized from Scheirer and Macdonald [47]. (c) Along-strike variation in crack density (i.e., the number of fissures per square kilometer of seafloor imaged with the *Argo I* video camera) after Wright et al. [7]. (d) Along-strike variation in relative axial lava age from Wright et al. [7]. Lava age criterion based on Haymon et al. [48]. (e) Along-strike variation in the number of hydrothermal vents actively discharging hydrothermal fluids in 1989 after Haymon et al. [48] and Wright et al. [7]. Fluid count includes high-temperature vents (black, white and gray smokers and smoke plumes) and low-temperature vents (milky or cloudy water). (f) Along-strike variation in average crack depth calculated using Model 2 with a preferred ν of 0.43. The seafloor and Layer 2A/2B boundary profiles are the same as in Fig. 5. Error bars represent the standard errors. Vertical exaggeration is 60 ×.

oldest, least hydrothermally active portions of the ridge crest where crack density is high. The widest cracks are found in the youngest lavas, and therefore are the youngest cracks. We suggest that these cracks are eruptive in origin and control the locations of high-temperature hydrothermal venting during the early stages of the volcanic–hydrothermal–tectonic cycle [7]. These cracks are wide, and hence deep, at the outset, and remain so until they are carried away from the neovolcanic zone by divergent plate motion. If their widths increased with time within the neovolcanic zone so would their depths, and eventually, at crustal depths of 500–800 m [14], the cracks would change into normal faults and thereby tend to close at the surface. In contrast to these sparse, young, hot cracks, the abundant, narrower, shallower cracks occurring in older, colder crust accumulate with time in response to tensile stresses. We suggest that these shallower cracks do not tap magma and are typically not hydrothermally active.

The direct proportionality of crack depth to crack width presented in this study adds to other observational evidence indicating that wide fissures in relatively young lava flows are primarily eruptive and are thus deep enough to tap melt. Recent *Alvin* observations confirm that many wide fissures in the study area appear to be eruptive in origin, and numerous high-temperature vents are localized along the margins of these wide fissures [42] (and Haymon et al., in prep.). Similar observations have been made on portions of the Juan de Fuca Ridge [45]. The most likely origin for these cracks is the inflation of the AMC due to the injection of melt from the upper mantle. In the magmatic pressure change model of Gudmundsson [46], magma accumulation and slight increases in magmatic pressure within the AMC prior to an eruption cause uplift and bending of the overlying crust, thereby generating tensile stress in the upper part of the crust that is sufficiently great to form cracks. During uplift and bending, the potential tensile stress is much higher than during ordinary divergent plate motion, resulting in cracks that may be exceptionally wide and deep.

There is a strong correlation between the greater depth of cracks at 9°42′–54′N and the location of the 1991 eruption of the ridge crest at ~9°45′–52′N [42]. The 1991 area of magmatic intrusion may extend as far south as 9°41′N based on the discovery of vapor-rich vents along fissures within the ASC during the 1991 *Alvin* AdVenture dive series. Haymon et al. [42] propose the intrusion of dikes to ~200 m beneath the floor of the ASC during the eruption, driving phase separation of hydrothermal fluids near the tops of the dikes and a large flux of vapor-rich fluids through the overlying rubbly lavas. The estimates of this study show that surficial cracks may penetrate deep enough to facilitate the flux of magma and fluids from the tops of the feeder dikes during an eruption event (in other words, an upward-propagating dike meets a downward-propagating crack).

The narrow, presumably shallow cracks (e.g., parts of Segment E and Segments F–G in Fig. 6) may be associated more with far-field plate stresses than with an inflated AMC. For example, on Segment F (Fig. 6) the cross-sectional area and topography of the ridge are significantly reduced compared to the ridge segments to the north and to Segment G to the south. The density of cracking and relative lava age are also significantly higher, and hydrothermal vent activity is virtually non-existent (Figs. 3 and 6).

Based on the observed correlation between cross-sectional area of the ridge axis (which may be thought of as a proxy for magmatic supply to the crust [47]), crack density, inferred crack depth, relative lava age, and hydrothermal vent abundance (Figs. 3 and 6), it is suggested that wide, presumably deep fissures in relatively young lava flows are primarily eruptive, and are loci for the formation of high-temperature hydrothermal vents above dike intrusions. Once dikes become emplaced in crust that is already subject to external tensile stress (related to divergent plate motion), there would be tensile stress concentration in portions of the crust directly above the vertical ends of these dikes that could easily form the wide cracks. Narrower, shallower fissures in relatively older lava flows are primarily tectonic in origin, forming in response to crustal extension. It is possible that some of these cracks form above dikes that are not as thick as those underlying the younger portions of the ridge crest. Dike thickness is proportional to driving pressure: the thicker the dike the greater the driving pressure, and the larger the crack [31]. Although all fissures provide pathways for seawater to enter the crust, which might potentially cool the hydrothermal and magmatic systems, it is sug-

gested that most hydrothermal heat loss in the axial zone occurs early along the wide, deep, eruptive fissures.

5. Conclusions

(1) The widest cracks are calculated to be the deepest cracks along EPR 9°12′–54′N. These cracks correspond to the broadest, youngest, and most hydrothermally active portions of the ridge crest where crack density is low [7,48]. The narrowest cracks are calculated to be the shallowest. These cracks correspond to the narrowest, oldest, and least hydrothermally active portions of the ridge crest where crack density is high [7,48].

(2) Wide cracks are calculated to be ~200–500 m deep (up to a maximum of ~1000 m deep), deep enough to reach the sheeted dike section (Layer 2B). These cracks may form due to enhanced tensile stresses arising from the inflation of the AMC, and thus have the most reasonable chance of being eruptive.

(3) Narrow, shallow cracks are presumably tectonic and form in response to crustal extension. It is also presumed that many of these cracks form above dikes that are not nearly as thick as those underlying the younger portions of the ridge crest.

(4) There is a strong correlation between the along-strike variation in depth of cracks at ~9°42′–54′N, based on *Argo I* mapping in 1989, and the location of the 1991 eruption of the ridge crest at 9°45′–52′N. Cracks in this region may have tapped melt during the eruption, as well as facilitated the flux of vapor-rich hydrothermal fluids through overlying lava flows. Wide, deep cracks are loci for the formation of high-temperature hydrothermal vents [42].

Acknowledgements

Many thanks to Agust Gudmundsson, Allan Rubin and Dan Fornari for helpful and encouraging discussions during the early stages of this research. The critical reviews of Agust Gudmundsson, Roger Buck, Graham Kent, Dan Scheirer and Doug Wilson significantly improved the manuscript. This research was supported by Office of Naval Research grants N00014-90-J1645 and N00014-93-10108, and National Science Foundation grants OCE-88-17587 and SES-88-10917. D.J.W. was also supported by the Ford Foundation. [*CL*]

References

[1] J. Geertsma and R. Haafkens, A comparison of the theories for predicting width and extent of vertical hydraulically induced fractures, J. Energy Resour. Technol. 101, 8–19, 1979.

[2] J.C. Jaeger and N.G.W. Cook, Fundamentals of Rock Mechanics, 3rd Ed., Chapman and Hall, London, 1979.

[3] M.H. Edwards, D.J. Fornari, A. Malinverno, W.B.F. Ryan and J. Madsen, The regional tectonic fabric of the East Pacific Rise from 12°50′N to 15°10′N, J. Geophys. Res. 96, 7995–8018, 1991.

[4] S. Carbotte and K.C. Macdonald, East Pacific Rise 8°–10°30′N: Evolution of ridge segments and discontinuities from SeaMARC II and three-dimensional magnetic studies, J. Geophys. Res. 97, 6959–6982, 1992.

[5] K.C. Macdonald, P.J. Fox, S. Carbotte, M. Eisen, S. Miller, L. Perram, D. Scheirer, S. Tighe and C. Weiland, The East Pacific Rise and its flanks, 8°–17°N: History of segmentation, propagation and spreading direction based on SeaMARC II and Sea Beam studies, Mar. Geophys. Res. 14, 299–334, 1992.

[6] P. Gente, J.M. Auzende, V. Renard, Y. Fouquet and D. Bideau, Detailed geological mapping by submersible of the East Pacific Rise axial graben near 13°N, Earth Planet. Sci. Lett. 78, 224–236, 1986.

[7] D.J. Wright, R.M. Haymon and D.J. Fornari, Crustal fissuring and its relationship to magmatic and hydrothermal processes on the East Pacific Rise crest (9°12′–54′N), J. Geophys. Res., in press.

[8] H.P. Johnson, Tectonic regulation of the physical properties of the seafloor: The view from the Juan de Fuca Ridge, in: Proc. Workshop Physical Properties of Volcanic Seafloor, G.M. Purdy and G.J. Fryer, eds., pp. 55–72, Woods Hole Oceanogr. Inst., Woods Hole, Mass., 1990.

[9] A.H. Lachenbruch, Depth and spacing of tension cracks, J. Geophys. Res. 66, 4273–4292, 1961.

[10] G.M. Purdy and G.J. Fryer, Proc. Workshop Physical Properties of Volcanic Seafloor, 279 pp., Woods Hole Oceanogr. Inst., Woods Hole, Mass., 1990.

[11] S.E. Harris and R.D. Ballard, ARGO: Capabilities for Deep Ocean Exploration, 69 pp., Mar. Technol. Soc., IEEE, Washington, D.C., 1986.

[12] J.-C. Sempéré and K.C. Macdonald, Overlapping spreading centers: Implications from crack growth simulation by the displacement discontinuity method, Tectonics 5, 151–163, 1986.

[13] D.D. Pollard and A. Aydin, Propagation and linkage of oceanic ridge segments, J. Geophys. Res. 89, 10017–10028, 1984.
[14] A. Gudmundsson and K. Bäckström, Structure and development of the Sveinagja Graben, Northeast Iceland, Tectonophysics 200, 111–125, 1991.
[15] A.M. Rubin, Dike-induced faulting and graben subsidence in volcanic rift zones, J. Geophys. Res. 97, 1839–1858, 1992.
[16] H. Tada, P.C. Paris and G.R. Irwin, The Stress Analysis of Cracks Handbook, 383 pp., Del Res. Corp., Hellertown, Penn., 1973.
[17] M.D. Zoback and R.N. Anderson, Ultrasonic borehole televiewer investigation of oceanic crustal layer 2A, Costa Rica Rift, Nature 295, 375, 1982.
[18] P.R. Shaw, Age variations of oceanic crust Poisson's ratio: Inversion and a porosity evolution model, J. Geophys. Res. 99, 3057–3066, 1994.
[19] N.I. Christensen, Ophiolites, seismic velocities and oceanic crustal structure, Tectonophysics 47, 131–157, 1978.
[20] G.L. Christeson, G.M. Purdy and G.J. Fryer, Seismic constraints on shallow crustal emplacement processes at the fast-spreading East Pacific Rise, J. Geophys. Res. 99, 17957–17996, 1994.
[21] O.I. Diachok, R.L. Dicus and S.C. Wales, Elements of a geoacoustic model of the upper crust, J. Acoust. Soc. Am. 75, 324–334, 1984.
[22] A.J. Harding, J.A. Orcutt, M.E. Kappus, E.E. Vera, J.C. Mutter, P. Buhl, and T.M. Brocher, Structure of young oceanic crust at 13°N on the East Pacific Rise from expanding spread profiles, J. Geophys. Res. 94, 1989.
[23] E.E. Vera, J.C. Mutter, P. Buhl, J.A. Orcutt, A.J. Harding, M.E. Kappus, R.S. Detrick and T.M. Brocher, The structure of 0-to 0.2-m.y.-old oceanic crust at 9°N on the East Pacific Rise from expanded spread profiles, J. Geophys. Res. 95, 15529–15556, 1990.
[24] P.M. Shearer, Cracked media, Poisson's ratio and the structure of the upper oceanic crust, Geophys. J. R. Astron. Soc. 92, 357–362, 1988.
[25] C.H. Cheng and D.H. Johnston, Dynamic and static moduli, Geophys. Res. Lett. 8, 39–42, 1981.
[26] A. Gudmundsson, Stress estimates from the length/width ratios of fractures, J. Struct. Geol. 5, 623–626, 1983.
[27] A. Gudmundsson, Emplacement of dikes, sills, and crustal magma chambers at divergent plate boundaries, Tectonophysics 176, 257–275, 1990.
[28] T. Forslund and A. Gudmundsson, Crustal spreading due to dikes and faults in southwest Iceland, J. Struct. Geol. 13, 443–457, 1991.
[29] A. Nur, The origin of tensile fracture lineaments, J. Struct. Geol. 4, 31–40, 1982.
[30] Q.F. Li, S.H. Hu, B.M. Zhong and J.Q. Wei, A further study on the effect of crack depth and shape on fracture toughness, Eng. Fracture Mech. 39, 219–227, 1991.
[31] A.M. Rubin and D.D. Pollard, Origins of blade-like dikes in volcanic rift zones, in: Volcanism in Hawaii, Vol. 2, R.W. Decker, T.L. Wright and P.H. Stauffer, eds., pp. 1449–1470, U.S. Geol. Surv., Denver, Colo., 1987.
[32] A.M. Rubin, A comparison of rift-zone tectonics in Iceland and Hawaii, Bull. Volcanol. 52, 302–319, 1990.
[33] J.R. Lister and R.C. Kerr, Fluid-mechanical models of crack propagation and their application to magma transport in dykes, J. Geophys. Res. 96, 10049–10077, 1991.
[34] A.H. Lachenbruch, A simple mechanical model for oceanic spreading centers, J. Geophys. Res. 78, 3395–3417, 1973.
[35] A. Gudmundsson, Formation and growth of normal faults at the divergent plate boundary in Iceland, Terra Nova 4, 464–471, 1992.
[36] A.A. Griffith, Theory of rupture, in: Proc. 1st Int. Congr. Applied Mechanics, C.B. Biezeno and J.M. Burgers, eds., pp. 55–63, Waltman, Delft, 1924.
[37] J. Lin and E.M. Parmentier, Mechanisms of lithospheric extension at mid-ocean ridges, Geophys. J. 96, 1–22, 1989.
[38] G.M. Kent, A.J. Harding and J.A. Orcutt, Distribution of magma beneath the East Pacific Rise between the Clipperton Transform and the 9°17′N DEVAL from forward modeling of common depth point data, J. Geophys. Res. 98, 13945–13970, 1993.
[39] A.J. Harding, G.M. Kent and J.A. Orcutt, A multichannel seismic investigation of upper crustal structure at 9°N on the East Pacific Rise: Implications for crustal accretion, J. Geophys. Res. 98, 13925–13944, 1993.
[40] E.E. Vera and J.B. Diebold, Seismic imaging of oceanic layer 2A between 9°30′N and 10°N on the East Pacific Rise from two-ship wide-aperture profiles, J. Geophys. Res. 99, 3031–3042, 1994.
[41] G.M. Kent, A.J. Harding and J.A. Orcutt, Distribution of magma near the 9°03′N overlapping spreading center from forward modeling of common depth point data, J. Geophys. Res. 98, 13971–13995, 1993.
[42] R.M. Haymon, D.J. Fornari, K.L. von Damm, M.D. Lilley, M.R. Perfit, J.M. Edmond, W.C. Shanks, III, R.A. Lutz, J.B. Grebmeier, S. Carbotte, D. Wright, E. McLaughlin, E. Smith, N. Beedle and E. Olson, Volcanic eruption of the mid-ocean ridge along the East Pacific Rise crest at 9°45–52′N: 1. Direct submersible observations of seafloor phenomena associated with an eruption event in April, 1991, Earth Planet. Sci. Lett. 119, 85–101, 1993.
[43] A. Gudmundsson, Tectonics of the Thingvellir fissure swarm, SW Iceland, J. Struct. Geol. 9, 61–69, 1987.
[44] R.W. Embley and D.S. Wilson, Morphology of the Blanco transform fault zone, NE Pacific: Implications for its tectonic evolution, Mar. Geophys. Res. 14, 25, 1992.
[45] R.W. Embley and W.W. Chadwick, Jr., Volcanic and hydrothermal processes associated with a recent phase of seafloor spreading at the northern Cleft segment: Juan de Fuca Ridge, J. Geophys. Res. 99, 4741–4760, 1994.
[46] A. Gudmundsson, Geometry, formation and development of tectonic fractures on the Reykjanes Peninsula, southwest Iceland, Tectonophysics 139, 295–308, 1987.
[47] D.S. Scheirer and K.C. Macdonald, Variation in cross-sec-

tional area of the axial ridge along the East Pacific Rise: Evidence for the magmatic budget of a fast-spreading center, J. Geophys. Res. 98, 7871–7886, 1993.

[48] R.M. Haymon, D.J. Fornari, M.H. Edwards, S. Carbotte, D. Wright and K.C. Macdonald, Hydrothermal vent distribution along the East Pacific Rise crest (9°09′–54′N) and its relationship to magmatic and tectonic processes on fast-spreading mid-ocean ridges, Earth Planet. Sci. Lett. 104, 513–534, 1991.

[49] W.S.D. Wilcock, D.R. Toomey, G.M. Purdy and S.C. Solomon, The renavigation of Sea Beam bathymetric data between 9° and 10°N on the East Pacific Rise, Mar. Geophys. Res. 15, 1–12, 1993.

[50] K.D. Klitgord and J. Mammerickx, Northern East Pacific Rise: Magnetic anomaly and bathymetric framework, J. Geophys. Res. 87, 6725–6750, 1982.